Long-Time Conformational Transitions of Alanine Dipeptide in Aqueous Solution: Continuous and Discrete-State Kinetic Models

Dmitriy S. Chekmarev, Tateki Ishida, and Ronald M. Levy*

Department of Chemistry and Chemical Biology and BioMaPS Institute for Quantitative Biology, Rutgers, the State University of New Jersey, 610 Taylor Road, Piscataway, New Jersey 08854

We present an analysis of the thermodynamics, conformational dynamics, and kinetics of the solvated alanine dipeptide molecule. Solvation was treated in the framework of the OPLS/analytic generalized born with nonpolar interactions effective potential model. The effective free energy map was generated in a series of multiwindow umbrella sampling all-atom simulations using the weighted histogram analysis method. A Brownian dynamics approach was used to examine the room-temperature dynamics of the dipeptide. To emulate the realistic dynamics of conformational interconversions of the alanine dipeptide in water, the parameters that govern the time evolution of the reduced model were chosen to mimic the intermediate-time dynamics of a model which treats both the solute and the solvent explicitly. The characteristic time (mean first passage time) for the "fast" $C7_{eq} \rightarrow \alpha_R$ transition was found to be around 249 ps in good agreement with the results of previously reported studies. From an ensemble of microsecond Brownian dynamics trajectories we were able to numerically estimate with high statistical precision the mean transition time for the "slow" transition $\alpha_R \rightarrow C7_{ax}$, which was found to be approximately 11 ns. Conformational kinetics of the dipeptide was further analyzed by introducing a discrete-state kinetic model consisting of four states (α_R, $\beta/C5/C7_{eq}$, α_L, and $C7_{ax}$) and 12 rate constants, which reproduces the long-time behavior of the Brownian dynamics simulations. The simulations described here complement and help to motivate single-molecule spectroscopic studies of alanine dipeptide and other peptides in aqueous solution. The close correspondence established between the continuous dynamics and a discrete-state kinetic model provides a possible route for studying the long-time kinetic behavior of larger polypeptides using detailed all-atom effective potentials.

I. Introduction

Since the pioneering paper of Rossky and Karplus,[1] the alanine dipeptide molecule (*N*-acetyl-alanine-*N′*-methylamide), sketched in Figure 1, has served as a model system for many computational studies of biopolymer structure and dynamics.[2−13] Despite its simplicity, the molecule is able upon solvation to adopt all conformational angles observed for α helix and β strand motifs in proteins.[2,3] Although the structure and thermodynamics of this system have been well-characterized by theoretical methods and to a lesser extent experimentally,[14,15] the conformational kinetics of this molecule is not fully resolved. The effective potential energy surface of alanine dipeptide exhibits approximately five minima, and the exact number depends on the details of the effective potential model; a visual analysis of the projection of the potential surface onto the $\phi(C-N-C_\alpha-C)$ and $\psi(N-C_\alpha-C-N)$ backbone dihedral angles suggests many possible routes by which the molecule might interconvert among these minima. Previous studies of the conformational dynamics of alanine dipeptide have focused on the "fast" interconversion between the two stable states $C7_{eq}$ and α_R by a direct route involving a variation in the backbone ψ dihedral angle. In this work we provide a more complete analysis of the full conformational kinetics of the alanine dipeptide molecule. We have two goals in mind. First, we hope to provide benchmark simulation results for comparison with spectroscopic experiments[16−21] designed to probe heterogeneous
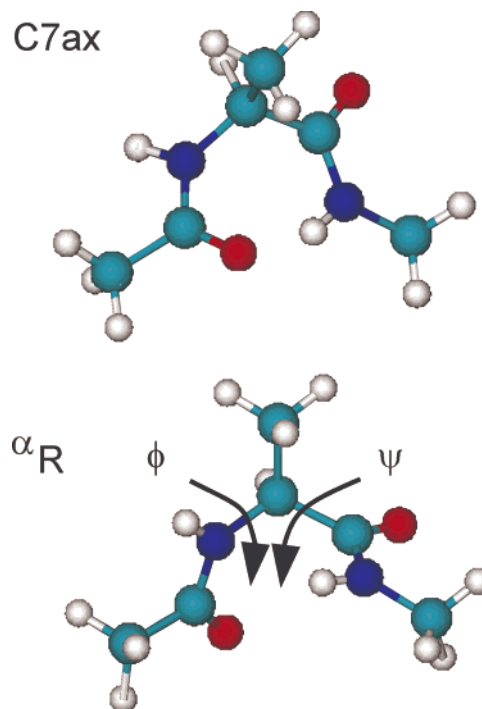
Figure 1. $C7_{ax}$ and α_R conformations of the alanine dipeptide molecule.

aspects of the conformational kinetics of peptides which are now beginning to be reported. Because the variation in the

* Corresponding author: e-mail ronlevy@lutece.rutgers.edu.

times required for transitions between the different minima spans several orders of magnitude (from picoseconds to arguably microseconds), we employ a recently developed implicit solvent effective potential[22] and use a Brownian dynamics (BD) algorithm to model the conformational transitions on this surface. While such a model does not include the specific effects of explicit waters in the dynamics, and these may be important for the kinetics,[10,12,14] with the current model we are able to explore alternative paths which connect each local minimum with the others, in a reasonable amount of computer time. Our second goal is to explore the correspondence that it is possible to establish between the continuous dynamics of alanine dipeptide in solution using a detailed atomic model and a simplified kinetic model for the long-time conformational transitions of this molecule.

Discrete kinetic models using highly simplified potentials have played an important role in the development of our understanding of the principles of protein folding.[23–31] Powerful numerical techniques for solving the corresponding master equations for these models can be used to explore their time evolution.[32,33] However, these simplified potentials lack atomic detail and their application to specific proteins is made difficult by their abstract nature. A current goal of the biophysical theory community is to develop hierarchical models for studying the conformational dynamics of peptides and proteins where the reduced models are derived in a consistent way from the more detailed ones. At the lowest level would be the fully atomic description of molecular dynamics (MD), including all the degrees of freedom of the peptide and the solvent. At an intermediate level of detail, the solvent degrees of freedom can be averaged over by introducing an implicit solvent effective potential and a Langevin equation of motion. There are many such examples in the literature (e.g., refs 9 and 34–39). Further reduction of the model complexity involves mapping the continuous dynamics on a physics-based effective potential onto a discrete-state model. Systematic approaches to this problem are lacking: the choice of states to use for the discretization of the continuous conformational dynamics, their construction, and the extraction of the corresponding kinetic parameters is not completely straightforward even for a molecular system as simple as alanine dipeptide in water. In this paper we construct "by hand" a discrete-state model for the alanine dipeptide conformational transitions consisting of 4 states and 12 rate constants which is consistent for longer times with the much more complicated BD of this molecule on the underlying implicit solvent effective potential. The discrete-state alanine dipeptide model provides a convenient framework for analyzing the large number of transition paths which together describe the dynamics of the alanine dipeptide molecule in solution.

In brief, our analysis consists of the following principal steps. After choosing backbone dihedral angles ϕ and ψ as conformational coordinates, the effective free energy map, or equivalently the potential of mean force (PMF), was constructed in a series of room-temperature umbrella sampling MD simulations, which sample all solute degrees of freedom, using the weighted histogram analysis method (WHAM).[40–42] Next, BD simulations were performed on this reduced surface. For our model to emulate the realistic conformational dynamics of alanine dipeptide in water, the parameters that govern the time evolution of such a reduced model were chosen to mimic the intermediate-time dynamics of a model which treats both the solute and the solvent explicitly. Characteristic transition times (mean first passage times) were evaluated from the histograms of the duration of all pertinent transition events that were recorded

during the entire course of the simulation. On the basis of the results of the BD simulations, we then examine the conformational dynamics of solvated alanine dipeptide in terms of a simple first-order kinetic model. This model describes the time evolution of the populations of several macrostates on the PMF surface representative of principal conformers of the alanine dipeptide molecule. This approach makes it possible to analyze quantitatively the entire spectrum of conformational transitions of the solvated alanine dipeptide molecule.

The paper is organized as follows. In section II, the method we used to map out the PMF is outlined. In section III, we examine the numerical algorithm for the reduced model BD. The results and discussion are presented in section IV.
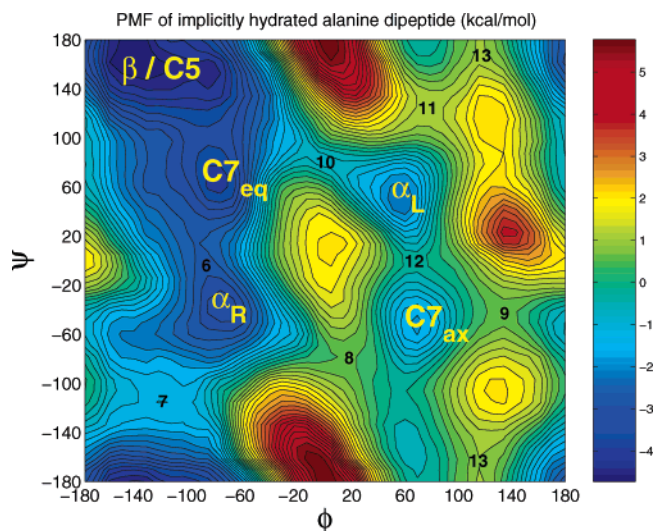
II. PMF of Alanine Dipeptide on the OPLS/Analytic Generalized Born with Nonpolar Interactions (AGBNP) Effective Potential Surface

The procedure we used to build the two-dimensional, in ϕ and ψ space, PMF of the hydrated alanine dipeptide molecule is given elsewhere.[43] Below we present a concise overview of the key steps taken.

We utilized a two-dimensional multiwindow umbrella sampling technique, the results of which were processed by the WHAM[40–42] to generate the effective free energy map. In umbrella sampling simulations, we used a regular grid of 19 × 19 = 361 windows for the conformational coordinate pairs varying from −180 to +180° in steps of 20° to which a second grid of 18 × 18 = 324 windows varying from −170 to +170° with the stepsize of 20° was added. For each window i the biasing potential was represented by a simple harmonic function $u_i(\phi, \psi) = 0.5k[(\phi - \phi_i)^2 + (\psi - \psi_i)^2]$ with the force constant being fixed at 250 kcal/(mol rad²). In total, 685 windows were organized to cover the entire conformational space ($-180 \leq \phi \leq +180°$, $-180 \leq \psi \leq +180°$). The MD simulations were carried out at 300 K with the solvent treated implicitly by the AGBNP effective potential model.[22] The OPLS-AA force field was employed to model the intramolecular potential.[44] Constrained minimization was used to prepare the starting configurations for the MD runs. After equilibrating for about 800 ps, 1.5-ns MD simulations using the RESPA[45] integrator as implemented in the IMPACT[46] software package were performed for each window to collect the data. The results were processed by the WHAM algorithm to produce the conformational distribution function $\mathscr{A}(\phi, \psi)$. The two-dimensional PMF was constructed according to $W(\phi, \psi) = -k_BT \ln \mathscr{A}(\phi, \psi)$ (determined to within an arbitrary constant).

To perform BD simulations, we need a method to compute numerically first (effective forces) and second (curvature effects) partial derivatives for any arbitrary point (ϕ, ψ) on the constructed PMF surface. For this purpose we used the cosine series modified Shepard bivariate interpolation routine of Renka and Brown.[47] This method yields C^2 interpolants, that is, with continuous second partial derivatives, and performs well on the analytical test surfaces with multiple intervening maxima and minima of moderate magnitude,[48] which resemble the PMF surface we have obtained for alanine dipeptide. A contour map of the interpolated PMF of alanine dipeptide on the OPLS/AGBNP effective potential surface is shown in Figure 2.

The main conformers of the hydrated alanine dipeptide molecule can be arranged in the following order according to the effective free energy difference ΔW with respect to the lowest energy structure $\beta/C5$:$\beta/C5$ (taken as zero energy) < $C7_{eq}$ ($\Delta W \approx 0.9$ kcal/mol) < α_R ($\Delta W \approx 1.5$ kcal/mol) < α_L

Conformational Transitions of Alanine Dipeptide

J. Phys. Chem. B, Vol. 108, No. 50, 2004 **19489**

Figure 2. Contour map of the interpolated PMF of the implicitly hydrated alanine dipeptide.

($\Delta W \approx 2.7$ kcal/mol) < $C7_{ax}$ ($\Delta W \approx 3.2$ kcal/mol). The ordering of the minima is not well resolved experimentally, but it was reported recently that the polyproline II, P_{II} ($\phi \approx -85°$, $\psi \approx 160°$), structure is the most stable conformer for alanine dipeptide in aqueous solution.[14] This structure is contained in the β/C5 pocket in the upper left quadrant of the PMF surface depicted in Figure 2. Comparison of the PMF in this study with the results of the QM/MM simulations of alanine dipeptide in water[13] as well as with the data from other MM simulations reported previously in the literature, as was summarized by Smith,[7] indicates that our model agrees reasonably well with the order in conformer stability of the hydrated alanine dipeptide molecule generally observed in all-atom simulations. In our model, α_L conformers are found to be slightly more stable (by about 0.5 kcal/mol) than the $C7_{ax}$ structures. This observation is consistent with the findings of recent QM/MM simulation studies.[13] In general, a net dipole moment of α-type dipeptide structures is largely responsible for the stabilization of these fragments in polar solvents.[2] In contrast, the minimization of intramolecular steric conflicts,[12] solute–solvent hydrogen bonding,[14] and higher conformational entropy are believed to be the main factors which contribute to the stabilization of extended structures (β/C5/C7) in solution.

Interestingly, the surface shown in Figure 2 matches fairly well the latest empirical $\phi - \psi$ Ramachandran diagram for nonrepetitive non-Gly, non-Pro, and non-pre-Pro protein structures constructed using a database of 500 high-resolution Protein Data Bank entities.[49] As can been seen by comparing Figure 2 with Figure 7 from ref 49, our model for the hydrated alanine dipeptide molecule PMF includes metastable minima in the lower right quadrant of the $\phi - \psi$ map, γ ($C7_{ax}$) and II′, using the terminology of ref 49, which have been observed experimentally in proteins.

III. Reduced Model BD Simulation

To probe the room temperature conformational dynamics of alanine dipeptide in water, the following first-order propagator was used to advance the system on the PMF surface generated as described in the previous section

$$\phi_{i+1} - \phi_i = \frac{D}{k_B T}\left(-\frac{\partial W(\phi, \psi)}{\partial \phi}\right)_{\phi=\phi_i} \Delta t + \sqrt{2D\Delta t}\omega_\phi$$

$$\psi_{i+1} - \psi_i = \frac{D}{k_B T}\left(-\frac{\partial W(\phi, \psi)}{\partial \psi}\right)_{\psi=\psi_i} \Delta t + \sqrt{2D\Delta t}\omega_\psi \quad (1)$$

with D being an effective diffusion coefficient and the ω's defining the random displacements along ϕ and ψ, which are sampled independently from a Gaussian distribution with unit variance and zero mean.[50] Our model assumes simple over-damped stochastic dynamics with the ϕ and ψ components of the random force being treated as Markovian.

This approach depends on a proper numerical choice for the diffusion coefficient D for reproducing the correct time scale. Recent studies[10,14] indicate that conformational dynamics of small peptides in solution may be sensitive to the structure of the nearest solvation shells which in turn may vary for different conformers. This implies that the diffusion coefficient should formally be regarded as a function of ϕ and ψ, that is, $D(\phi, \psi)$, which can, in principle, be deduced from the all-atom simulations. In the present work, we take a simpler approach and approximate $D(\phi, \psi)$ for the entire $W(\phi, \psi)$ surface by the constant value $D_\psi^{HK} = 0.15$ rad^2/ps, which was inferred by Hummer and Kevrekidis from the coarse MD analysis of the explicitly solvated alanine dipeptide.[11]

It should be noted that in writing eq 1 we have assumed that the force is constant during the time step and is determined by its value at the point (ϕ_i, ψ_i). Consequently, the time step cannot be made too large, otherwise this will result in unphysically fast dynamics. When the curvature effects are taken into account [but we still neglect higher order terms $O(\Delta t^2)$],[51] the following condition defines an upper limit on the time step for the numerical scheme expressed by eq 1[11,52]

$$\Delta t < \left(\frac{D}{k_B T}\left|\frac{\partial^2 W(\phi, \psi)}{\partial l^2}\right|\right)^{-1} \quad (2)$$

where the second directional derivative can be evaluated as

$$\left|\frac{\partial^2 W(\phi, \psi)}{\partial l^2}\right| = \left|\left(\frac{\partial^2 W}{\partial \phi^2}\right)\cos^2\theta + 2\left(\frac{\partial^2 W}{\partial \phi \partial \psi}\right)\cos\theta\sin\theta + \left(\frac{\partial^2 W}{\partial \psi^2}\right)\sin^2\theta\right| \quad (3)$$

In eqs 2 and 3, $\cos\theta = \Delta\phi/\Delta l = \Delta\phi/(\Delta\phi^2 + \Delta\psi^2)^{1/2}$ and $\sin\theta = \Delta\psi/\Delta l = \Delta\psi/(\Delta\phi^2 + \Delta\psi^2)^{1/2}$. It was found that for the time step $\Delta t = 0.1$ ps the number of steps that violate the condition of eq 2 always remains below 4%, which was taken by us as an acceptable error margin (such moves have not been actually discarded, but their effect on the final data is negligible).

The dynamics algorithm works as follows. In every BD run, we focus on transitions between each pair of minima on the PMF surface, say A and B. Each minimum i is represented geometrically by a segment on the $W(\phi, \psi)$ surface centered around the lowest for this particular conformer energy point W_i^{min} with the borders chosen such that all points within these limits energetically are no higher than $k_B T$ above W_i^{min}. The arbitrariness of such a classification does not influence significantly the dynamics of a system for which the effective energy surface is essentially a collection of distinct minima, each being surrounded by energy barriers of several $k_B T$ in magnitude. We measure the duration of each transition event; specifically, for each $A \rightarrow B$ transition we start the clock when the system arrives

TABLE 1: Dynamic Characteristics of Transitions between the C7$_{eq}$, the α$_R$, and the C7$_{ax}$ Conformers of the Hydrated Alanine Dipeptide from BD Simulations[a]

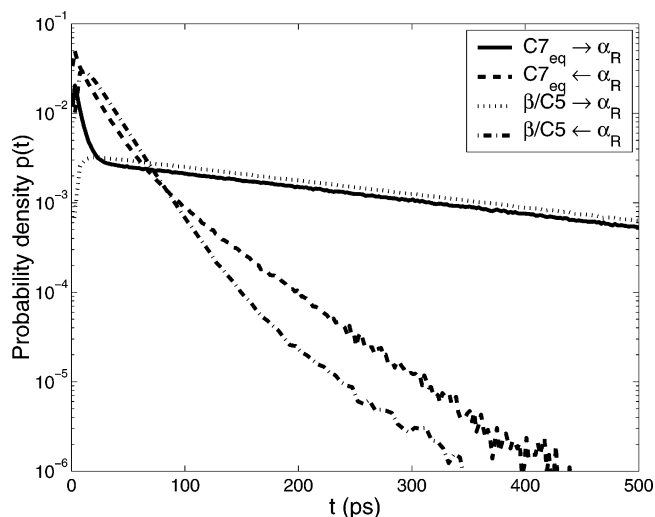| transition	N_{tr}[b]	$\langle t \rangle$ (mean first passage time)
C7$_{eq}$ → α$_R$	3608×10^3	249 ps
α$_R$ → C7$_{eq}$	3611×10^3	27 ps
β/C5 → α$_R$	3084×10^3	293 ps
α$_R$ → β/C5	3087×10^3	29 ps
α$_R$ → C7$_{ax}$	88×10^3	≈11 ns
C7$_{ax}$ → α$_R$	88×10^3	224 ps

[a] Relative error ≤5%. Consult Figure 2 for details. [b] Number of recorded transitions per millisecond.

at the region designating minimum A and record the time when it first reaches the domain of minimum B. The time difference gives us the duration of this particular transition event, that is, provides an estimate for the first passage time. The forward transition is followed by monitoring the backward transition $A \leftarrow B$, and the cycle repeats. To improve statistics, the algorithm runs simultaneously 1000 independent replicas of the BD simulation for time t_{sim}; that is, we are following the time evolution of an ensemble of 1000 independent Brownian particles each subject to the two-dimensional effective potential $W(\phi, \psi)$. At the end of the run, the recorded first passage times from all replicas are combined to build two histograms $H_f(t)$ (forward reaction) and $H_r(t)$ (backward reaction) for the corresponding transition events between minima A and B. These histograms are properly normalized so that $\sum_t H_{f,r}(t) = 1$. In particular, each bin t_n reflects the number of transition trajectories of duration $t_n \leq t < t_n + \delta t_{bin}$ divided by the total number of transitions counted for this particular transformation in the entire course of the simulation. The distributions are of similar shape. At short times[53] they increase rapidly from 0 to some maximum values and then they exhibit, to good approximation, an exponential or multiexponential decay. The characteristic transition time, or the mean first passage time, is evaluated as $\langle t \rangle_{f,r} = \sum_t t H_{f,r}(t) \approx \int_t t p_{f,r}(t) \, dt$, where $p_{f,r}(t) \approx H(t)_{f,r}/\delta t_{bin}$ approximates the probability density for completing the conversion from A to B or in the opposite direction, in time t. In addition, the occupation probability of state B for the reaction $A \rightarrow B$ (i.e., with absorbing boundary at B) at a certain time τ can be estimated as $P_B(\tau) = \sum^\tau H_f(t) = \int_0^\tau p_f(t) \, dt$. Finally, we note that the following relation $1000 t_{sim} \approx \langle t \rangle_f N_f + \langle t \rangle_r N_r$, where t_{sim} is the simulation time of the BD run and $N_{f,r}$ are the total numbers of the observed transition events for forward and reverse reactions for all 1000 replicas, is satisfied as can be verified using the data in Table 1.

IV. Results and Discussion

A. Mean First Passage Times and the Kinetics of Conformational Transitions. We start by considering the "fast" C7$_{eq}$ ⇌ α$_R$ conformational transitions. These transitions have been well-characterized in the literature.[3,7,10,11] Irrespective of the differences in the methods used including both the choice of the force field and the simulation algorithm, the mean transition times between this specific pair of conformers have been calculated to be in the picosecond range. We have carried out a series of room-temperature BD simulations to generate the histograms of the first passage times for the forward and backward reactions between C7$_{eq}$ and α$_R$. The resulting first passage time probability densities are shown on a semilog scale in Figure 3.

The mean first passage time for the C7$_{eq}$ → α$_R$ reaction was found to be 249 ps, and the corresponding time for the reverse

Figure 3. First passage time distributions (probability densities) for transitions between the C7$_{eq}$, the β/C5, and the α$_R$ conformations of the hydrated alanine dipeptide. C7$_{eq}$ → α$_R$ (solid). C7$_{eq}$ ← α$_R$ (dashed). β/C5 → α$_R$ (dotted). β/C5 ← α$_R$ (dashed−dotted). The 0−500 ps segment of $p(t)$ is shown.

reaction C7$_{eq}$ ← α$_R$ was estimated to be 27 ps. The analysis of transition trajectories revealed that transitions over the barrier 6 (consult Figure 2) constitute the dominant route that accounts for about 84% of all C7$_{eq}$ → α$_R$ transition trajectories, while approximately 13% of the total number follow the roundabout path C7$_{eq}$ ⇌ β/C5 $\overset{7}{\rightarrow}$ α$_R$. Other possible routes are hardly sampled at all, for instance, less than 3% of all generated C7$_{eq}$ → α$_R$ trajectories take the C7$_{eq}$ → α$_L$ → C7$_{ax}$ → α$_R$ route. Because of the strong energetic downward slope toward the global minimum structure β/C5 and the small barrier ($<k_B T$) separating C7$_{eq}$ from β/C5, most trajectories which originate in the C7$_{eq}$ domain are forced to explore the β/C5 region and undergo several interconversions between C7$_{eq}$ and β/C5 before eventually surmounting barrier 6 to convert into the α$_R$ conformer. Only about 17% of the recorded transitions proceed directly from C7$_{eq}$ over the barrier 6 into α$_R$ without first visiting the β/C5 domain. The existence of direct and indirect paths for transitions is reflected in the biexponential character of the computed first passage time distribution $P_f(t)$ for C7$_{eq}$ → α$_R$ (Figure 3). In addition, we have examined the dynamics of transitions between the β/C5 and the α$_R$ conformations. We estimate $\langle t \rangle_f \approx 293$ ps for β/C5 → α$_R$ and $\langle t \rangle_r \approx 29$ ps for β/C5 ← α$_R$. Transitions over barrier 6 again dominate, accounting for ~81% of all observed β/C5 → α$_R$ transition trajectories, whereas the fraction of trajectories following the alternative route via transition region 7 increases slightly to about 16%. Naturally, now it takes more time for the system to approach the barrier 6 before converting into α$_R$. This is reflected in the difference visible in the short-time domain 0−50 ps between the distribution of the β/C5 → α$_R$ first passage times and the one describing the C7$_{eq}$ → α$_R$ transformations as can be seen in Figure 3. The results are summarized in Table 1. All together, our results conform to the previous observations that isomerization between C7$_{eq}$ and α$_R$ structures is largely restricted to variation of the ψ torsion angle alone.[2,3,10,11] However, we also find an alternative pathway C7$_{eq}$ ⇌ β/C5 $\overset{7}{\rightarrow}$ α$_R$ accounting for ~13% of the C7$_{eq}$ → α$_R$ transitions which was neglected in previous studies.

Now we analyze the results obtained for the "slow" transition α$_R$ → C7$_{ax}$. The only available estimate for the mean transition time between these two conformers is due to Smith,[7] who

Conformational Transitions of Alanine Dipeptide

*J. Phys. Chem. B, Vol. 108, No. 50, 2004* **19491**
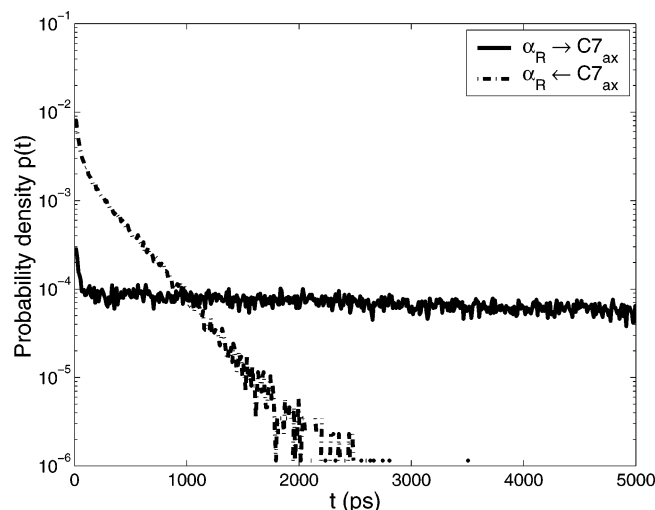
Figure 4. First passage time distributions (probability densities) for transitions between the α_R and the $C7_{ax}$ conformations of the hydrated alanine dipeptide. $\alpha_R \rightarrow C7_{ax}$ (solid). $\alpha_R \leftarrow C7_{ax}$ (dashed–dotted). The 0–5 ns segment of $p(t)$ is shown.

Figure 5. Snapshot of a typical $\alpha_R \rightarrow C7_{ax}$ transition trajectory proceeding via the α_L state. Every 10th step of the trajectory is shown.


Figure 6. Snapshot of a typical $\alpha_R \rightarrow C7_{ax}$ transition trajectory proceeding over the barrier 8. Every 10th step of the trajectory is shown.

estimated that it would take about 2.5 μs for the α_R structure to make a transition to the $C7_{ax}$ conformation. This estimate was made by analyzing the relative heights of the effective energy barriers in their potential model (CHARMM in explicit solvent) which separate the α_R and $C7_{ax}$ structures rather than by generating the transitions directly.[7] Our results, from room-temperature BD simulations on the OPLS/AGBNP effective potential surface with the reduced model, yield a faster transition time, with $\langle t \rangle_f \approx 11$ ns and $\langle t \rangle_r \approx 224$ ps (Table 1). The respective distributions of the first passage times are shown in Figure 4. They are in qualitative agreement with the finding of Derreumaux and Schlick,[9] who found that the $C7_{ax}$ state had been sampled in the 20-ns Langevin dynamics simulations that they performed. As evident in Figure 2, there are several structurally significant routes available for a trajectory started at the α_R minimum to reach the $C7_{ax}$ state. For instance, the conversion can be accomplished either by "direct" transitions $\alpha_R \rightarrow C7_{ax}$ via barriers 8 and 9 or the system may opt for an "indirect" path $\alpha_R \rightarrow \beta/C5/C7_{eq} \xrightarrow{10} \alpha_L \xrightarrow{12} C7_{ax}$. The "direct" route corresponds to the burst phase in the $\alpha_R \rightarrow C7_{ax}$ first passage time distribution in Figure 4. However, the majority of trajectories take the indirect path; this is discussed in the following section. We find that close to 98% of the recorded transition trajectories for $\alpha_R \rightarrow C7_{ax}$ did at some point visit the $\beta/C5$ state on the OPLS/AGBNP effective potential surface. Furthermore, the analysis of residence time reveals that about 91% of the total simulation period t_{sim} the system spends in the PMF region encompassing $\beta/C5$ and $C7_{eq}$ states. The corresponding fractions for states α_R, α_L, and $C7_{ax}$ are, respectively, 3, 0.23, and 0.13%. These numbers correlate very well with relative equilibrium populations estimated from the shape of the PMF surface (i.e., from the ratio of the composite Boltzmann factors evaluated for the corresponding regions on the PMF surface). Figure 5 and 6 serve to illustrate the fact that a typical $\alpha_R \rightarrow C7_{ax}$ transition trajectory can be locked for an extended period of time in the region which encloses the three lowest energy states: $\beta/C5$, $C7_{eq}$, and α_R. The observed behavior is suggested by the shape of the PMF with $\beta/C5$ being the absolute minimum, with the $C7_{eq}$ potential minimum being within $\sim 1.5 k_B T$, and with the potential barrier heights among the $\beta/C5$, $C7_{eq}$, and α_R structures being within $\sim 3 k_B T$. This confirms the
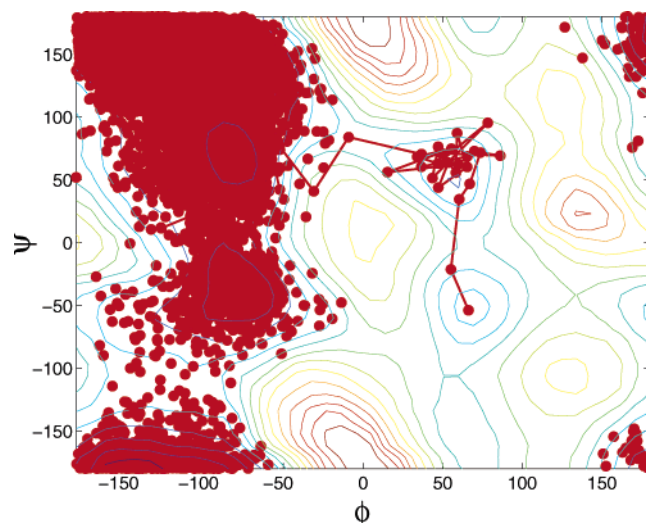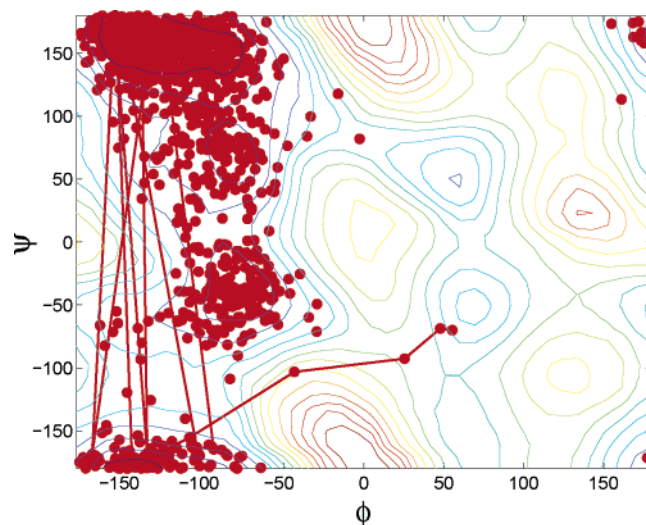
importance of the $\beta/C5$ structure as the dominant intermediate for interconversion between the α_R and $C7_{ax}$ conformers.

Finally, in concluding this section we note that it was recently demonstrated by Yeh and Hummer that the shear viscosity of the TIP3P water is smaller than the experimental value by a factor of 2.87.[54] Because in this study we have used an effective diffusion coefficient extracted from all-atom MD simulations which utilized the TIP3P water model,[11] the reported mean first passage times may be underestimated. Under the assumption that the computed mean first passage times scale linearly with the solvent viscosity,[50] the modified times would be $\langle t \rangle \approx 700$ ps for $C7_{eq} \rightarrow \alpha_R$, $\langle t \rangle \approx 80$ ps for $C7_{eq} \leftarrow \alpha_R$, $\langle t \rangle \approx 30$ ns for $\alpha_R \rightarrow C7_{ax}$, and $\langle t \rangle \approx 640$ ps for $\alpha_R \leftarrow C7_{ax}$.

B. Discrete-State Kinetic Model and the Master Equation. For illustration, and to connect with our analysis of the first passage times above, we consider the irreversible passage of the alanine dipeptide from the initial state α_R to the final state $C7_{ax}$. We employ a kinetic scheme which connects all of the most frequently visited macrodomains (discrete states) on the PMF. The BD simulations indicate that the appropriate states to consider are α_R, α_L, $C7_{ax}$, and $\beta/C5/C7_{eq}$, with the last one being formed by combining the domains of $\beta/C5$ and $C7_{eq}$, an approximation that in the discrete-state kinetics context is
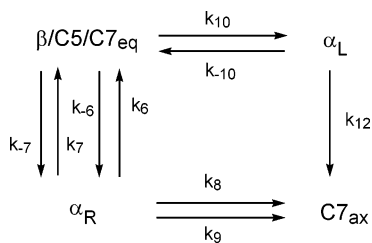
Figure 7. Kinetic model describing the irreversible transfer of population from α_R to $C7_{ax}$.

TABLE 2: Values of Rate Constants and Average Barrier Heights for the Kinetic Scheme Sketched in Figure 7[a]

rate constant	in ps^{-1}	$\Delta W/k_B T$[b]
k_8	1/2025	6.26
k_{-8}	1/132	3.53
k_9	1/2425	6.44
k_{-9}	1/158	3.71
k_6[c]	1/36	2.23
k_{-6}	$1/(s \times 328) = 1/1181$	4.44
k_7	1/136	3.56
k_{-7}	$1/(s \times 1111) = 1/4000$	5.66
k_{10}	$1/(s \times 2150) = 1/7740$	6.32
k_{-10}	1/104	3.29
k_{12}	1/105	3.3
k_{-12}	1/54	2.63

[a] Plotted in Figures 8−10, solutions were obtained with the conformational area scaling factor $s = 3.6$. [b] Room temperature $k_B T = 0.596$ kcal/mol. [c] Reference transition with k estimated directly from BD simulations.

suggested by the results of BD simulations (see discussion in section IV.A). Then, the irreversible transfer of population from α_R to $C7_{ax}$ can be represented by the first-order kinetic scheme shown in Figure 7, which transforms into the following set of coupled constant coefficient ordinary differential equations

$$
\begin{cases}
\dfrac{dP_{\alpha_R}}{dt} = -(k_6 + k_7 + k_8 + k_9)P_{\alpha_R} + (k_{-6} + k_{-7})P_{\beta/C5/C7_{eq}} \\[2mm]
\dfrac{dP_{\beta/C5/C7_{eq}}}{dt} = (k_6 + k_7)P_{\alpha_R} - (k_{-6} + k_{-7} + k_{10})P_{\beta/C5/C7_{eq}} + k_{-10}P_{\alpha_L} \\[2mm]
\dfrac{dP_{\alpha_L}}{dt} = k_{10}P_{\beta/C5/C7_{eq}} - (k_{-10} + k_{12})P_{\alpha_L} \\[2mm]
\dfrac{dP_{C7_{ax}}}{dt} = (k_8 + k_9)P_{\alpha_R} + k_{12}P_{\alpha_L}
\end{cases} \tag{4}
$$

where $P_i(t)$ denotes the probability for the system to occupy state i at time t. The above system of equations must be solved subject to the initial conditions $P_{\alpha_R}(0) = 1$ and $P_{\beta/C5/C7_{eq}}(0) = P_{\alpha_L}(0) = P_{C7_{ax}}(0) = 0$.

We use a TST-like approach to estimate the single step rate constants which enter the kinetic model specified above. This is suggested by the overall shape of the effective potential surface, for which the assigned states are isolated from each other by energy barriers of more than $2k_B T$ (refer to data in Table 2). Thus, we can express rate constants for the transitions between state i and state j in the Arrhenius form[55,56,50] $k_{ij} = A_i e^{-\Delta W_i/k_B T} = A_i e^{-(W^{\ddagger}-W_i)/k_B T}$ and $k_{ji} = A_j e^{-\Delta W_j/k_B T} = A_j e^{-(W^{\ddagger}-W_j)/k_B T}$, where $W^{\ddagger}$ is the height of the effective barrier between i and j. Each pre-exponential factor A_i is proportional to the ratio of the conformational area ascribed to the transition (barrier) region and that of the domain corresponding to the minimum i on the PMF surface. To generate sensible estimates for the rate

constants in eq 4 we used the following procedure. First, we noticed that the fast $\alpha_R \rightarrow C7_{eq}$ isomerization reaction can be adequately approximated by a two-state kinetic model involving two parallel routes: crossing over barriers 6 and 7, respectively. Direct evaluation of the $\alpha_R \xrightarrow{6} C7_{eq}$ rate by counting trajectories in BD simulations yielded $k_6 = 1/36$ ps^{-1}. Other rates were then found by appropriate rescaling of the energetic (exponential) and the entropic (pre-exponential) contributions to k_6. In doing this, we have assumed that conformational areas of all transition regions are the same and that the areas occupied by the minima at α_R, α_L, and $C7_{ax}$ do not differ significantly from each other. For example, we estimated $k_7 = 1/136$ ps^{-1} and, hence, $\langle t \rangle = 1/(k_6 + k_7) \approx 28.5$ ps, which agrees well with the value of 27 ps computed for the $\alpha_R \rightarrow C7_{eq}$ transition directly from the simulations (Table 1). To account for a large conformational area associated with the $\beta/C5/C7_{eq}$ state, we have introduced a scaling factor s, which is a measure of how much bigger this area is with respect to the one sampled on average by the α_R structure. The scaling factor s is essentially the only adjustable parameter in our kinetic model. The resulting values are collected in Table 2. Because the rate of escape from $\beta/C5/C7_{eq}$ over the barrier $13 k_{13} \approx 1/24\,674$ ps^{-1} (Figure 2) is much smaller than other escape rates from this particular conformation, this route has not been incorporated into the model.

The system of equations (eq 4) has been solved numerically[57] with different values of the scaling factor s. Qualitatively, analysis of the conformational areas sampled by the trajectories (refer, for example, to Figures 5 and 6) implies that s is between 3 and 4. It was found that for $s = 3.6$ very good correspondence is observed between the distribution of first passage times computed from the BD simulations and the one resulting from the discrete-state kinetics analysis. The probability density $p(t)$ of the latter is given by the last equation in eq 4. The solutions for the discrete kinetic model with $s = 3.6$ are shown in Figures 8 and 9 together with the results from the continuous BD simulations. The fit of the four-state kinetic model to the BD simulations of first passage times between α_R and $C7_{ax}$ is very good over 3 orders of magnitude in time. At short times, the biexponential character of $p(t)$ for $\alpha_R \rightarrow C7_{ax}$ can be clearly seen in Figure 8 (lower panel). The so-called "burst phase" is attributed to those trajectories which transform directly from α_R into the $C7_{ax}$ structure without visiting the $\beta/C5/C7_{eq}$ domain. This happens at the initial stage of the $\alpha_R \rightarrow C7_{ax}$ reaction and is reflected in the high initial rate of population increase of the $C7_{ax}$ state (upper panel of Figure 9). The fraction of such transitions is very small, though; it is given by the area under the corresponding segment of the $p(t)$ curve in Figure 8 and amounts to only a few percent of the total number of transitions. This is perfectly consistent with the BD simulations finding that only about 2% of the $\alpha_R \rightarrow C7_{ax}$ transition trajectories do not visit the $\beta/C5/C7_{eq}$ state. The majority of the $\alpha_R \rightarrow C7_{ax}$ transitions proceed through formation of the $\beta/C5/C7_{eq}$ intermediates. They finally arrive at $C7_{ax}$ by either crossing over barriers 8 and 9 or by choosing the $\beta/C5/C7_{eq} \xrightarrow{10} \alpha_L \xrightarrow{12} C7_{ax}$ route (lower panel of Figure 9). The time spent sampling the minima corresponding to $\alpha_R \rightleftharpoons \beta/C5/C7_{eq}$ ($\rightleftharpoons \alpha_L$) defines the overall time scale of this conformational isomerization reaction.

The eigenvalues and eigenvectors of the four-state kinetic model (eq 4 and Figure 7) for the alanine dipeptide conformational transitions are listed in Table 3. The dominating time scale of the $\alpha_R \rightarrow C7_{ax}$ isomerization reaction can be extracted from the lowest nonvanishing eigenvalue. In particular, in a two-state approximation to $\alpha_R \rightarrow C7_{ax}$ the overall rate constant k

Conformational Transitions of Alanine Dipeptide

J. Phys. Chem. B, Vol. 108, No. 50, 2004 **19493**

(a)

(b)
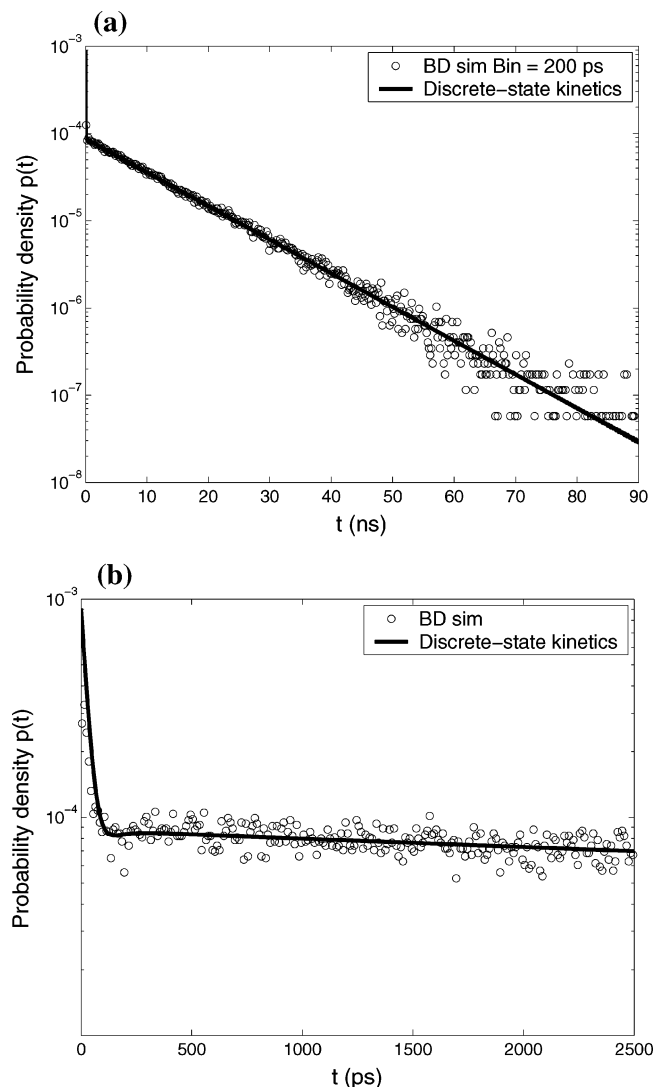
Figure 8. First passage time distributions (probability densities) for transitions $\alpha_R \rightarrow C7_{ax}$. Upper panel: BD simulations (circles) with the time bin size 200 ps. Discrete-state kinetics (solid line). Lower panel: BD simulations (circles) with the time bin size 10 ps. Discrete-state kinetics (solid line). The $0-2.5$ ns segment of $p(t)$ is shown.

for population transfer is $k \approx |\mathbf{Re}\lambda|$,[56] where λ is the smallest nonvanishing eigenvalue of the rate matrix $\mathbf{K}$ for system 4 $[\mathrm{d}\mathbf{P}(t)/\mathrm{d}t = \mathbf{KP}(t)]$. We have calculated $|\lambda| \approx 0.0001$ ps^{-1}, and the mean escape time $\tau = 1/|\mathbf{Re}\lambda| \approx 10$ ns, which agrees very well with the value obtained in BD simulations (Table 1). Note that the smallest nonvanishing eigenvalue is 2 orders of magnitude smaller than the largest eigenvalue; this much faster relaxing mode corresponds to the rapid equilibration that occurs between α_R and $\beta/C5/C7_{eq}$. A component analysis of the eigenvector corresponding to the lowest nonzero eigenvalue confirms that the $\beta/C5/C7_{eq}$ state is the most populated "intermediate", while the nonequilibrium population of α_L is the smallest. Even so, as discussed below, the majority of trajectories which begin in α_R and end in $C7_{ax}$ pass through α_L.

The discrete-state kinetics analysis can be used to obtain information about the relative importance of alternative routes for the transition $\alpha_R \rightarrow C7_{ax}$. We have computed and compared the instantaneous fluxes into the $C7_{ax}$ state from the adjacent α_R and α_L states: $j_{\alpha_R}(t) = (k_8 + k_9)P_{\alpha_R}(t)$ and $j_{\alpha_L}(t) = k_{12}P_{\alpha_L}(t)$, respectively. The short-time behavior of $j_{\alpha_R}(t)$ and $j_{\alpha_L}(t)$ is illustrated in Figure 10. Initially, we observe $j_{\alpha_R}(t) >$


(a)

(b)
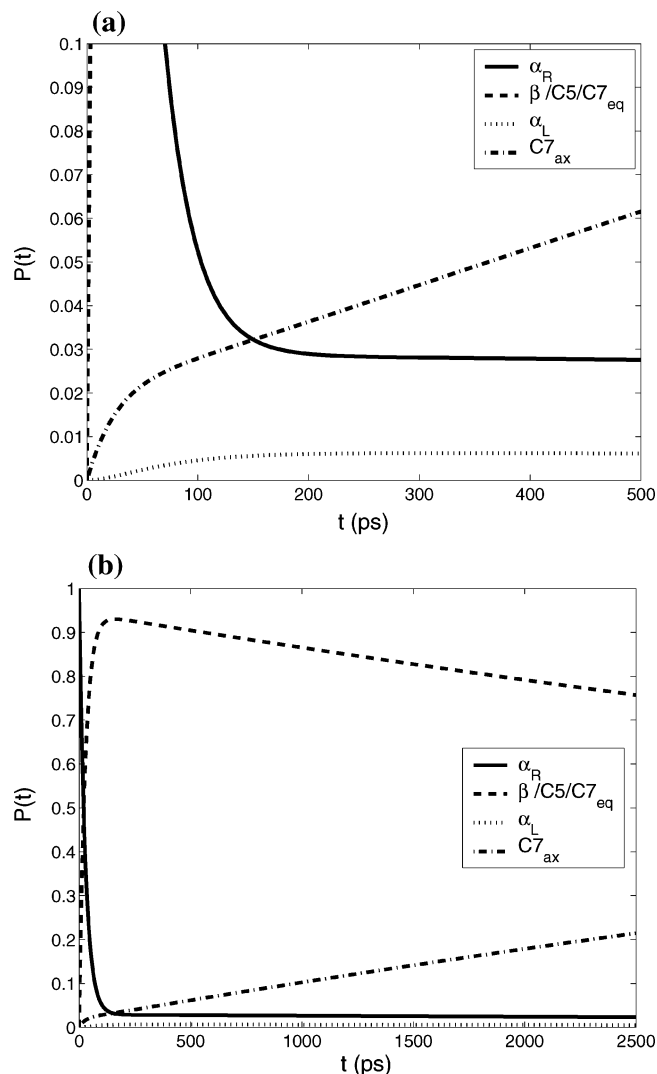
Figure 9. Upper panel: incipient stages of state population dynamics for the discrete-state kinetic model depicted in Figure 7. Lower panel: state population dynamics for the discrete-state kinetic model depicted in Figure 7.

TABLE 3: Eigenvalues and Components of the Corresponding Eigenvectors of the Rate Matrix K (eq 4) for the Four-State Kinetic Model Displayed in Figure 7

eigenvalue (ps^{-1})	$|\lambda_1| = 0$	$|\lambda_2| \approx 0.0001$	$|\lambda_3| \approx 0.0192$	$|\lambda_4| \approx 0.0371$
α_R	0	0.0212	0.0255	-0.7138
$\beta/C5/C7_{eq}$	0	0.6939	0.3913	0.7001
α_L	0	0.0047	-0.8246	-0.0050
$C7_{ax}$	1.0	-0.7198	0.4078	0.0187

$j_{\alpha_L}(t)$, but for $t \geq 120$ ps the flux from the α_L state starts to dominate. At $t \geq 50$ ns due to the irreversibility of the kinetic scheme (Figure 7) the magnitude of either flux diminishes to a negligible value. The fraction of the transition trajectories following each of these paths into $C7_{ax}$ is given by $n_i = \int j_i(t)$ dt $(\sum_i n_i = 1)$. Numerical integration of the flux curves yielded $n_{\alpha_L} \approx 0.68$ and $n_{\alpha_R} \approx 0.32$. This is consistent with the results of BD simulations that imply that the likelihood of getting to $C7_{ax}$ via the final-stage transition $\alpha_L \xrightarrow{12} C7_{ax}$ is higher than that for transitions following $\alpha_R \xrightarrow{8,9} C7_{ax}$. The flux analysis highlights the fact that a nonequilibrium intermediate present at low concentration (α_L) may still define the dominant path between initial and final states, although this is not immediately obvious from an eigenvector component analysis alone. This
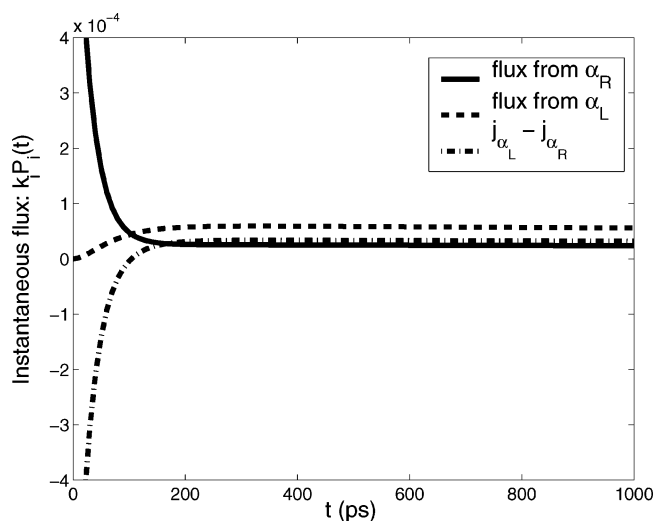
Figure 10. Instantaneous fluxes $j_{\alpha_R}(t) = (k_8 + k_9)P_{\alpha_R}(t)$ and $j_{\alpha_L}(t) = k_{12}P_{\alpha_L}(t)$.

observation may prove to be useful for modeling more complex polypeptides using simple kinetic schemes as has been reported recently.[30,31]

Finally, to verify that the simplified four-state kinetic model does reproduce the equilibrium properties of the alanine dipeptide OPLS/AGBNP effective potential surface, we have modified the kinetic scheme in Figure 7 to account for the decay out of the C7$_{ax}$ state by introducing additional rate constants k_{-8}, k_{-9}, and k_{-12} evaluated as was described earlier in the text. We should recover in the limit of long times ($t \rightarrow \infty$) the equilibrium populations of the specified macro states. Indeed, the equilibrium results for the modified kinetic scheme contain the following relative populations: 95.7% for β/C5/C7$_{eq}$, 3% for α_R, 1% for α_L, and 0.3% for C7$_{ax}$. These data are in good agreement with the results of the residence time analysis of BD simulations as well as the static population analysis based on the shape of the PMF surface.

V. Conclusions

In this paper we have presented an analysis of the thermodynamics, conformational dynamics, and kinetics of the alanine dipeptide molecule in aqueous solution. Solvation was treated in the framework of the OPLS/AGBNP implicit solvation effective potential model.[22] A BD approach was used to model the dynamics of the peptide backbone ϕ and ψ coordinates on the PMF constructed from all-atom simulations of the solute on the effective potential surface. The characteristic time scales for the motions span 5 orders of magnitude from the subpicosecond thermal fluctuations of the peptide backbone to the transitions among stable and metstable states on the time scale of tens of nanoseconds. Our focus has been on constructing a discrete-state kinetic model which is consistent with the underlying BD derived from the physics-based effective potential. An analysis of the simulations suggests a kinetic model containing 4 states and 12 elementary rate constants. The model can be used to explain quantitatively the multiexponential first passage time distributions of more complicated transitions involving multiple paths, such as the transitions between the α_R and the C7$_{ax}$ conformations which involve several different paths, each with significant population density. Interestingly, while the eigenvectors of the master equations provide information about the relative concentrations of intermediates along the "reaction path", they do not provide direct information about

which is the dominant path. To determine the most important paths, an analysis of reactive fluxes is needed. Finally, we note that single-molecule spectroscopy is providing new insights into the kinetics of confomationally heterogeneous systems.[16−18,20] Recently hidden Markov models have been introduced to extract rates directly from single-molecule photon arrival trajectories.[21] This approach is well-suited for determining rate constants for conformational transition within a framework like the kinetic scheme used here to model BD of alanine dipeptide in solution. By combining computer simulations of the dynamics of peptides based on all-atom effective potential models with the corresponding single-molecule experiments, we hope that it will be possible to achieve a more complete and consistent picture of the motions of these molecules over a large range of time scales.

References and Notes

(1) Rossky, P. J.; Karplus, M. *J. Am. Chem. Soc.* **1979**, *101*, 1913.
(2) Brooks, C. L., III; Case, D. *Chem. Rev.* **1993**, *93*, 2487.
(3) Smith, P. E.; Pettitt, B. M.; Karplus, M. *J. Phys. Chem.* **1993**, *97*, 6907.
(4) Apostolakis, J.; Ferrara, P.; Caflisch, A. *J. Chem. Phys.* **1999**, *110*, 2099.
(5) Anderson, A. G.; Hermans, J. *Proteins: Struct., Funct., Genet.* **1988**, *3*, 262.
(6) Tobias, D. J.; Brooks, C. L., III. *J. Phys. Chem.* **1992**, *96*, 3864.
(7) Smith, P. E. *J. Chem. Phys.* **1999**, *111*, 5568.
(8) Wu, X.; Wang, S. *J. Phys. Chem. B* **1998**, *102*, 7238.
(9) Derreumaux, P.; Schlick, T. *Proteins: Struct., Funct., Genet.* **1995**, *21*, 282.
(10) Bolhuis, P.; Dellago, C.; Chandler, D. *Proc. Natl. Acad. Sci. U.S.A.* **2000**, *97*, 5877.
(11) Hummer, G.; Kevrekidis, I. G. *J. Chem. Phys.* **2003**, *118*, 10762.
(12) Drozdov, A. N.; Grossfield, A.; Pappu, R. V. *J. Am. Chem. Soc.* **2004**, *126*, 2574.
(13) Hu, H.; Elstner, M.; Hermans, J. *Proteins: Struct., Funct., Genet.* **2003**, *50*, 451.
(14) Weise, C. F.; Weisshaar, J. C. *J. Phys. Chem. B* **2003**, *107*, 3265.
(15) Lavrich, R. J.; Plusquellic, D. F.; Suenram, R. D.; Fraser, G. T.; HightWalker, A. R.; Tubergen, M. J. *J. Chem. Phys.* **2003**, *118*, 1253.
(16) Weiss, S. *Nat. Struct. Biol.* **2000**, *7*, 724.
(17) Lipman, E. A.; Schuler, B.; Bakajin, O.; Eaton, W. A. *Science* **2003**, *301*, 1233.
(18) Yang, H.; Luo, G.; Karnchanaphanurach, P.; Louie, T. M.; Rech, I.; Cova, S.; Xun, L.; Xie, X. S. *Science* **2003**, *302*, 262.
(19) Woutersen, S.; Mu, Y.; Stock, G.; Hamm, P. *Proc. Natl. Acad. Sci. U.S.A.* **2001**, *98*, 11254.
(20) Talaga, D. S.; Lau, W. L.; Roder, H.; Tang, J.; Jia, Y.; DeGrado, W. F.; Hochrasser, R. M. *Proc. Natl. Acad. Sci U.S.A.* **2000**, *97*, 13021.
(21) Andrec, M.; Levy, R. M.; Talaga, D. S. *J. Phys. Chem. A* **2003**, *107*, 7454.
(22) Gallicchio, E.; Levy, R. M. *J. Comput. Chem.* **2004**, *25*, 479.
(23) Sali, A.; Shakhnovich, E. I.; Karplus, M. *J. Mol. Biol.* **1994**, *235*, 1614.
(24) Abkevich, V. I.; Gutin, A. M.; Shakhnovich, E. I. *Biochemistry* **1994**, *33*, 10026.
(25) Shakhnovich, E. I. *Curr. Opin. Struct. Biol.* **1997**, *7*, 29.
(26) Dinner, A.; Sali, A.; Smith, L. J.; Dobson, C. M.; Karplus, M. *Trends Biochem. Sci.* **2000**, *25*, 331.
(27) Kolinski, A.; Skolnick, J. *Proteins* **1994**, *18*, 338.
(28) Klimov, D. K.; Thirumalai, D. *J. Mol. Biol.* **1998**, *282*, 471.
(29) Muñoz, V.; Henry, E. R.; Hofrichter, J.; Eaton, W. A. *Proc. Natl. Acad. Sci. U.S.A.* **1998**, *95*, 5872.
(30) Ozkan, S. B.; Dill, K. A.; Bahar, I. *Protein Sci.* **2002**, *11*, 1958.
(31) Ozkan, S. B.; Dill, K. A.; Bahar, I. *Biopolymers* **2003**, *68*, 35.

(32) Van Kampen, N. G. *Stochastic processes in physics and chemistry*; North-Holland: Amsterdam, 1992.

(33) Zwillinger, D. *Handbook of differential equations*; Academic Press: San Diego, 1992.

(34) Levy, R. M.; Karplus, M.; McCammon, J. A. *Chem. Phys. Lett.* **1979**, *65*, 4.

(35) Klimov, D. K.; Thirumalai, D. *Phys. Rev. Lett.* **1997**, *79*, 317.

(36) Klimov, D. K.; Thirumalai, D. *Proc. Natl. Acad. Sci. U.S.A.* **2000**, *97*, 2544.

(37) Shen, T.; Wong, C. F.; McCammon, J. A. *J. Am. Chem. Soc.* **2001**, *123*, 9107.

(38) Kostov, K. S.; Freed, K. F. *Biophys. J.* **1999**, *76*, 149.

(39) Shen, M. y.; Freed, K. F. *Biophys. J.* **2002**, *82*, 1791.

(40) Ferrenberg, A. M.; Swedsen, R. H. *Phys. Rev. Lett.* **1989**, *63*, 1195.

(41) Kumar, J.; Bouzida, D.; Swedsen, R. H.; Kollman, P.; Rosenberg, J. M. *J. Comput. Chem.* **1992**, *13*, 1011.

(42) Kumar, J.; Rosenberg, J. M.; Bouzida, D.; Swedsen, R. H.; Kollman, P. *J. Comput. Chem.* **1995**, *16*, 1339.

(43) Ishida, T.; Levy, R. M. Manuscript in preparation.

(44) Jorgensen, W. L.; Maxwell, D. S.; Tirado-Rives, J. *J. Am. Chem. Soc.* **1996**, *118*, 11225.

(45) Tuckerman, M.; Berne, B. J.; Martyna, G. J. *J. Chem. Phys.* **1992**, *97*, 1990.

(46) *IMPACT*; Schrödinder: Portland, OR.

(47) Renka, R. J.; Brown, R. *ACM Trans. Math. Software* **1999**, *25*, 74.

(48) Renka, R. J.; Brown, R. *ACM Trans. Math. Software* **1999**, *25*, 78. We followed the recommendations of Renka and Brown and kept $N_c = 18$ and $N_w = 32$ throughout the course of the dynamics simulations.

(49) Lovell, S. C.; Davis, I. W.; Arendall, B. W., III; de Bakker, P. I. W.; Word, M. J.; Prisant, M. G.; Richardson, J. S.; Richardson, D. C. *Proteins: Struct., Funct., Genet.* **2003**, *50*, 437.

(50) Zwanzig, R. *Nonequilibrium Statistical Mechanics*; Oxford University Press: New York, 2001.

(51) Alternatively, a second-order scheme such as the stochastic Runge–Kutta technique can be implemented instead of eq 1. Higher order methods allow larger time steps because the force is evaluated several times (at least twice) per time step and, thus, its variation during the time step is better approximated. See, for instance, ref 52 and references therein.

(52) Branka, A. C.; Heyes, D. M. *Phys. Rev. E* **1999**, *60*, 2381.

(53) Initial rapid increase of $H_{f,r}(t)$ may not always be visible because of low resolution of the histogram with δt_{bin} normally exceeding several picoseconds.

(54) Yeh, I. C.; Hummer, G. *J. Am. Chem. Soc.* **2002**, *124*, 6563.

(55) Karplus, M. *J. Phys. Chem. B* **2000**, *104*, 11.

(56) Hänngi, P.; Talkner, P.; Borkovec, M. *Rev. Mod. Phys.* **1990**, *62*, 251.

(57) The initial value problem was solved using the MATLAB ode45 solver. Matching results were obtained in the eigenvalue/eigenfunction expansion analysis. Consult, for example, ref 33.

(58) Swope, W. C.; Pitera, J. W.; Suits, F. *J. Phys. Chem. B* **2004**, *108*, 6571.

(59) Swope, W. C.; Pitera, J. W.; Suits, F.; Pitman, M.; Eleftheriou, M.; Fitch, B. G.; Germain, R. S.; Rayshubski, A.; Ward, T.; Zhestkov, Y.; Zhou, R. *J. Phys. Chem. B* **2004**, *108*, 6582.